Analysis of Slanted Air-gap Structure of Interior Permanent Magnet Synchronous Motor with Brushless Field Excitation

Seong Taek Lee [1]
Student Member, IEEE
[1]University of Tennessee
414 Ferris Hall
Knoxville, TN 37996, USA
slee10@utk.edu

Leon M. Tolbert [1,2]
Senior Member, IEEE
[2]Oak Ridge National Laboratory
2360 Cherahala Boulevard
Knoxville, TN 37932, USA
tolbert@utk.edu

[*]*Abstract* -- **This paper introduces a new air-gap structure, the slanted air-gap, for increasing the speed limit of an interior permanent magnet synchronous motor (IPMSM) for application in a hybrid electric vehicle. This unique slanted air-gap is intended to maximize the ratio of the back-emf of a machine that is controllable by brushless field excitation (BFE). The BFE structure offers high torque per ampere per core length at low speed and weakened flux at high speed. Although the irregularly shaped air-gap reduces the air-gap flux, it also makes a flux barrier along the d-axis flux path and decreases the d-axis inductance. Therefore, the reluctance torque of the machine increases to compensate for the decreased permanent magnet torque; as a result, the machine achieves a higher ratio of the magnitude of controllable back-emf without losing the high torque capability resulting from the BFE.**

***Index Terms*— air gaps, inductance, permanent magnet machine, synchronous motors, torque.**

I. NOMENCLATURE

BFE	brushless field excitation
IPMSM	interior permanent magnet synchronous motor
FEA	finite element analysis
PM	permanent magnet

II. INTRODUCTION

The interior permanent magnet synchronous motor (IPMSM) is currently used by many leading auto manufacturers for hybrid electric vehicles because the power density for this type of motor is high compared with induction motors and switched reluctance motors. However, the primary drawback of the IPMSM is the limited high-speed operation caused mainly by the high back-emf from the permanent magnets (PM) and the low d-axis inductance value [1]–[2].

To avoid the primary drawbacks of the IPMSM, a brushless field excitation (BFE) structure is introduced [3]–[6]. This structure offers two advantages: (1) high torque per ampere per core length at low speed as a result of using flux, which is enhanced by increasing DC current to a fixed excitation coil, and (2) flux, which is weakened at high speed by reducing current to the excitation coil.

The ratio of the magnitude of the back-emf between the lowest and the highest excited condition is an important factor for developing the IPMSM with BFE. For this purpose, a slanted air-gap structure is analyzed. Although the irregularly shaped air-gap reduces the air-gap flux, it also makes a flux barrier only on the d-axis flux path and decreases the d-axis inductance. Additionally, the overall waveform of the reluctance torque versus input phase current angle will be shifted from 135° to 90° which is the angle of the maximum PM torque position. Therefore, the total output torque of the machine could increase to compensate for the decreased PM torque; as a result, the machine achieves a higher ratio of the magnitude of controllable back-emf without losing the high torque capability that results from the BFE.

III. THEORETICAL APPROACH TO SLANTED AIR-GAP

Without considering the cross-coupled flux linkage between the d- and q- axes, the reluctance torque equation is expressed as [7] –[10]

$$T_r = \frac{m}{2} p\left(L_d - L_q\right) i_d i_q = \frac{m}{2} p\left(\lambda_{d,id} i_q - \lambda_{q,iq} i_d\right) \qquad (1)$$

where m is the number of phase conductors, p is the number of pole pairs, L is inductance, and i is the instantaneous current. The subscripts d and q indicate the d-axis and q-axis, respectively. In the right side of (1), $\lambda_{d,id}$ is the d-axis flux linkage caused by d-axis current, and $\lambda_{q,iq}$ is the q-axis flux linkage caused by q-axis current. Since the total output torque is determined by mainly q-axis current, the reluctance torque will be increased when $\lambda_{d,id}$ is small and $\lambda_{q,iq}$ is high. Slanted air-gap is considered for this purpose.

Fig. 1 shows the example rotor with the slanted air-gap. The solid lines in the figure are the original d- and q-axis when the rotor has a uniform air-gap. To increase the reluctance torque, the new d- and q- axis will be rotated with the angle of α, as shown by the dashed line in Fig. 1. Then, the new reluctance torque equation will be

[*] The submitted manuscript has been authored by a contractor of the U. S. Government under contract no. DE-AC05-00OR22725. Accordingly, the U.S. Government retains a nonexclusive, royalty-free license to publish or reproduce the published form of this contribution, or allow others to do so, for U. S. Government purposes. Research sponsored by the Oak Ridge National Laboratory managed by UT-Battelle, LLC for the U. S. Department of Energy under contract DE-AC05-00OR22725.

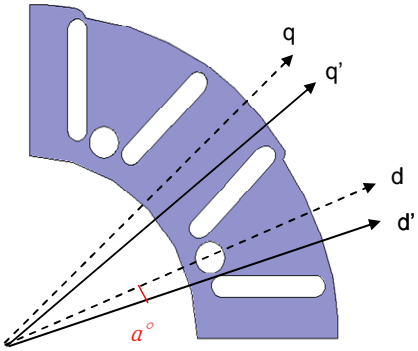

Fig. 1. Example rotor with slanted air-gap.

$$T_r = \frac{m}{2} p\left(L_{d'} - L_{q'}\right) i_{d'} i_{q'} = \frac{m}{2} p\left(L_{d'} - L_{q'}\right) i_{d+\alpha} i_{q+\alpha} \qquad (2)$$

Since the PM flux is sufficiently strong and the rotor has a wide neutral space between the north and south poles, the original d-q axis for the PM flux will be shifted slightly. Assuming that q-axis flux linkage is relatively small in the sine-distributed winding machine, the overall output torque equation is

$$\begin{aligned} T &= \frac{m}{2} p\left(\lambda_{d,PM} i_q + \left(L_{d'} - L_{q'}\right) i_{d+\alpha} i_{q+\alpha}\right) \\ &= \frac{m}{2} p\left(\lambda_{d,PM} I \sin\theta + \left(L_{d'} - L_{q'}\right) I^2 \sin 2(\theta+\alpha)\right) \end{aligned} \qquad (3)$$

where θ is the current angle with respect to the +d-axis on the current d-q plane, and I is the peak current . Equation (3) indicates that the maximum value of the reluctance torque will be shifted from 135° toward 90° with the angle of α as illustrated in Fig. 2. Fig. 2 also shows that the maximum value of the total output torque is little changed, although the slanted air-gap has lower PM torque.

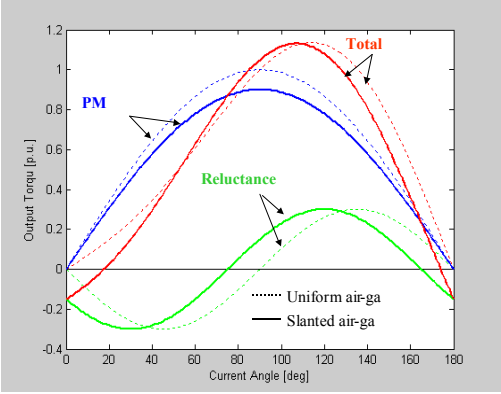

Fig. 2. Expected output torque of slanted air-gap in Fig. 1.

IV. FEA Simulation for Comparison

The theoretical approach to slanted air-gap structure can be ascertained by FEA simulation. Fig. 3 shows three different rotor models with the same permanent magnet arrangement, stator shape, and BFE. The rotor in Fig. 3 (a) has an ordinary air-gap width, 0.74 mm (0.029 inches); the rotor in (b) has non-uniform air-gap width between the permanent magnets, the deepest air-gap width is 2 mm (0.079 inches); and the rotor in (c) has slant air-gap shape, gap width varies from 2.54 mm (0.1 inches) to 0.74 mm (0.029 inches). Each model has the same air-gap length on the q-axis at 0.74 mm, but on the d-axis the length is different; 0.74 mm for (a), 2 mm for (b), and variable distance for (c).

The increased distance of the air-gap aids in blocking the d-axis magnetic flux flowing from stator to rotor or reverse but does not affect significantly the q-axis. This results in higher saliency ratio and increased reluctance torque. Fig. 4 shows the simulation results that the reluctance torque is increased for the case of the non-uniform or slant air-gap rotor compared with the torque of the rotor with uniform air-gap. As expected in theoretical approach, in the case of the slant air-gap rotor, the angle position of maximum torque is shifted toward 90° which is the position at which maximum torque is achieved without reluctance torque.

For this reason, the maximum torque position of the slant air-gap rotor is also shifted toward 90° as shown in Fig. 5. Therefore, the peak value of the maximum torque of the slant air-gap rotor is almost the same as that of the uniform air-gap rotor in spite of the lack of air-gap flux. This characteristic is one of the advantages of the slanted air-gap IPMSM because the iron loss will be decreased at the same output torque operation for reduced flux density from the rotor.

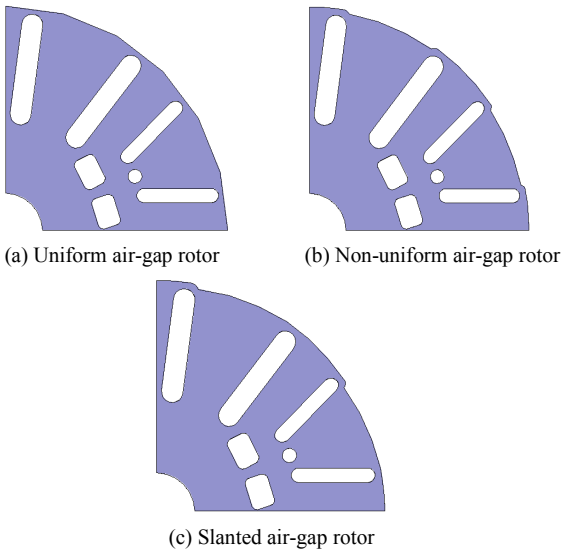

(a) Uniform air-gap rotor (b) Non-uniform air-gap rotor

(c) Slanted air-gap rotor

Fig. 3. Three different basic rotor shapes for FEA.

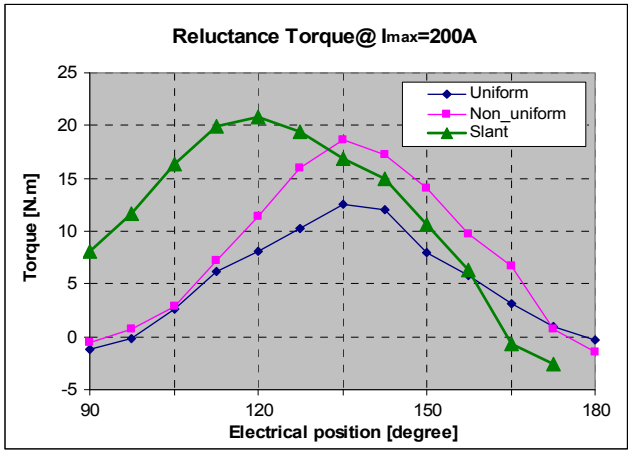

Fig. 4. FEA simulation results of the reluctance torque of each model.

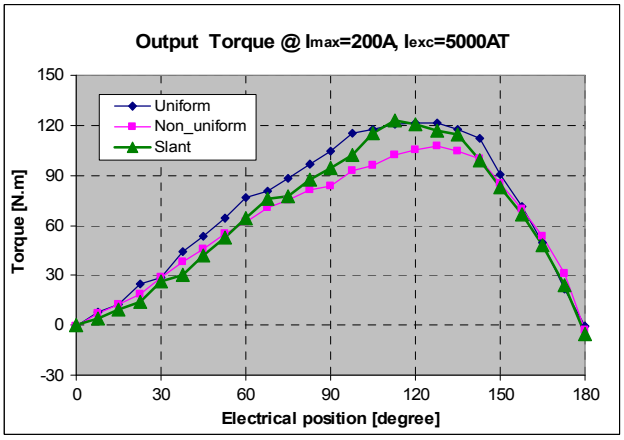

Fig. 5. FEA simulation results of the output torque of each model.

Originally, the concept of the slanted air-gap shape is for increasing the controllable back-emf ratio without losing the high torque capability of the machine. The controllable back-emf is enabled by a unique side-PM structure and side-field excitation coils that produce axial flux. This flux is added to the main flux from the PMs inside the rotor and interacts with the stator current to produce motor torque. The details are presented in [3], [4], and [6].

Fig. 6 is the simulation results of the air-gap flux density distributions for each air-gap model. Each model was simulated in three different excited conditions: 0 AT, 3000 AT, and 5000 AT. With a higher excited current, each model has higher air-gap flux. In other words, by the benefit of the DC excitation structure, the air-gap flux density is altered by changing the DC excitation current as shown in Fig. 6. Especially, if the air-gap flux can be reduced as much as possible, the machine can be operated at high speed operation, which is one of the weaknesses of an IPMSM [1]–[2].

Also, the iron loss will be significantly decreased in the high speed operation because this loss is proportional to the

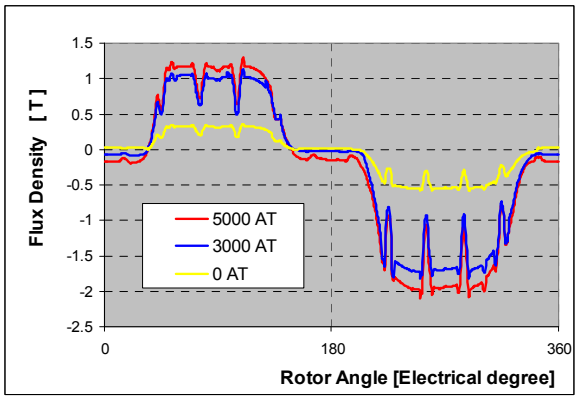

(a) Uniform air-gap rotor

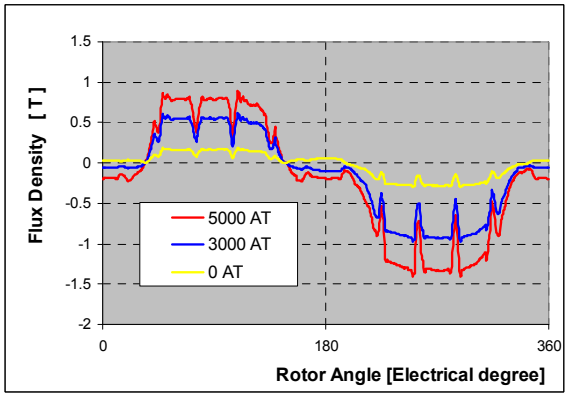

(b) Non-uniform air-gap rotor

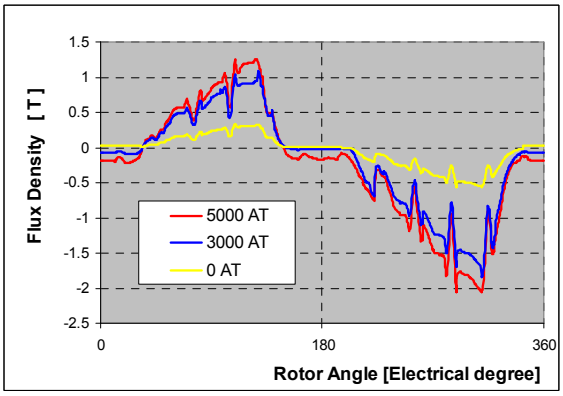

(c) Slanted air-gap rotor

Fig. 6. Simulation results of the air-gap flux density distributions.

square of the value of the flux density. For this reason, a higher value of the back emf ratio between the highest and the lowest excitation condition is desirable because this ratio is directly related to the value of the controllable air-gap flux.

Table I summarizes simulation results for the output performance of each motor for different excitation conditions: 0 AT and 5000 AT. In this table, PM torque means the calculation results of the output torque when the torque angle is 90°. At this load condition, the reluctance torque should be nearly zero for uniform and non-uniform

air-gap rotor models, but in the case of the slant air-gap rotor, the reluctance torque will be included because of its characteristics of shifting reluctance torque as shown in Fig. 4. Table I shows that the slanted air-gap rotor has a higher back-emf ratio than the uniform air-gap rotor despite the similar output torque performances, which is a desired characteristic for BFE. In case of the non-uniform air-gap rotor, the expected output torque is significantly reduced compared with the expected value of uniform air-gap rotor although it has the highest ratio among three types of the air-gap shape.

TABLE I
Comparison of simulation results in different air-gap models

Excitation current		Uniform	Non-uniform	Slant
0 AT	PM torque	33.22 Nm	27.97 Nm	29.18 Nm
	Max. torque	45.19 Nm	37.78 Nm	40.54 Nm
	Back -emf *	97.1 V	62.8 V	73.9 V
5000 AT	PM torque	104.59 Nm	84.14 Nm	92.22 Nm
	Max.torque	121.51 Nm	107.31 Nm	123.09 Nm
	Back- emf *	219.8 V	172.2 V	181.3 V
Back-emf ratio between 0 AT and 5000 AT		2.26	2.74	2.45

* at 5000 rpm

V. Experimental Results

After investigating various slanted air-gap shapes, the prototype has its slanted air-gap in 2.54 mm (0.1 inches) of the maximum depth and a half span width between two vertical PMs inside the rotor. Fig. 7 shows the assembled rotor core stack of the prototype motor.

The assembled prototype of the Oak Ridge National Laboratory (ORNL) 16,000-rpm motor design is shown in Fig. 8. This ORNL motor has a unique side-PM structure and side-field excitation coils to control the amount of the air-gap flux using the axial flux from side as mentioned in section IV. Table II compares the dimensions of the ORNL 16,000-rpm motor with those of a Toyota Prius motor that was selected as a baseline motor.

Fig. 9 is the expected reluctance torque of the prototype motor when the input phase current is 200 A (I_{max}=200A). In the figure, the analysis results of the slanted air-gap motor (prototype) are compared with the motor without slanted air-gap structure (uniform air-gap rotor). The analytical results in this analysis are obtained from the magnetic equivalent circuit considering the excitation flux from the axial side. The details are presented in [11].

Fig. 9 shows that the slanted air-gap structure has a higher maximum value of reluctance torque in both analytical and FEA methods (42.98 Nm vs. 15.73 Nm in analytical method, and 35.92 Nm vs. 12.57 Nm in FEA method). Also, the maximum torque position is shifted from 135° toward 90° as desired. For its increased reluctance torque, the slanted air-gap rotor can achieve higher output torque than the uniform air-gap rotor as shown in Fig. 10.

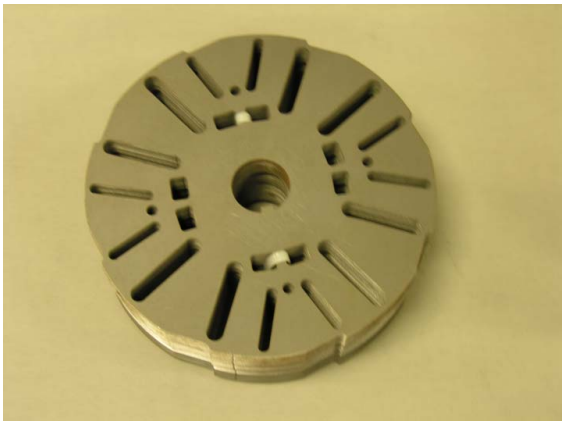

Fig. 7. Assembled rotor core stack.

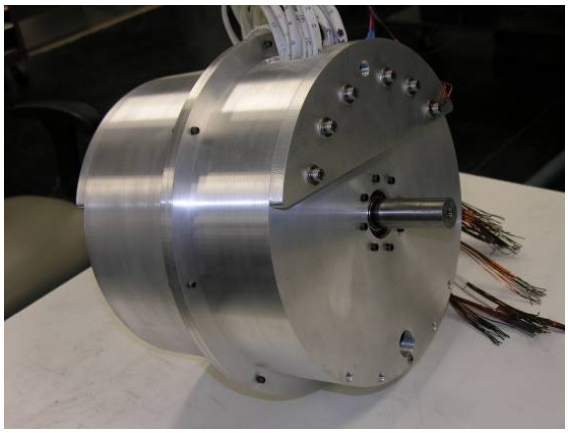

Fig. 8. Assembly of ORNL 16,000-rpm motor.

TABLE II
Comparison of Dimensions of the ORNL 16,000-rpm Motor and the Baseline Motor

	Prius	**ORNL**
Speed	6,000 rpm	16,000 rpm
Stator lamination outer diameter	269.2 mm	269.2 mm
Rotor outer diameter	160 mm	160 mm
Core length	83.82 mm	47.75 mm
Bearing to bearing outer face	196.85 mm	189.23 mm
Magnet weight	1.25 kg	1.16 kg
Estimated field adj. ratio	none	2.5
Rating	33/50 kW	33/50 kW
Boost converter	yes	no
High-speed core loss	high	low

Fig. 10 is the expected output torque profile when input phase current is 200 A and the excitation current is 5 A (I_{exc}=5A). Since the excitation coils are wound 865 turns, the total excitation condition is 4325 AT. The experimental test results are also plotted in Fig. 10, which are agreeable to the analysis results. Fig. 11 is another comparison plot when the input phase current is 50 A. The experimental results are not much different from the analysis results of both equivalent circuit and FEA. Fig. 11 also shows that the maximum torque position approaches to 90° like the pattern in Fig. 10 when the input phase current is 200 A.

Fig. 12 is the experimental results showing the controllable back emf voltage. The baseline waveforms in Fig. 12 are obtained at 1,000 rpm with no field excitation and enhanced by a field excitation of +5A. These graphs prove that the back emf voltage can be controllable by the excitation current.

Table III indicates the effect of the slanted air-gap in both output torque and back emf ratio. Although there is some difference between FEA simulation and experimental test results, it is clear that the slanted air-gap rotor has higher output torque and controllable back emf ratio.

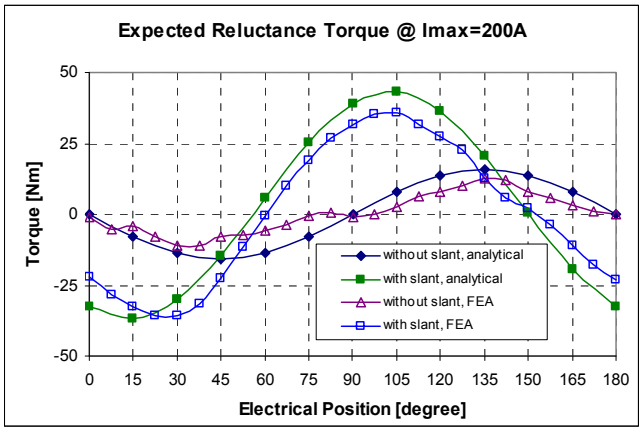

Fig. 9. Comparison of the expected reluctance torque at I_{max}=200A.

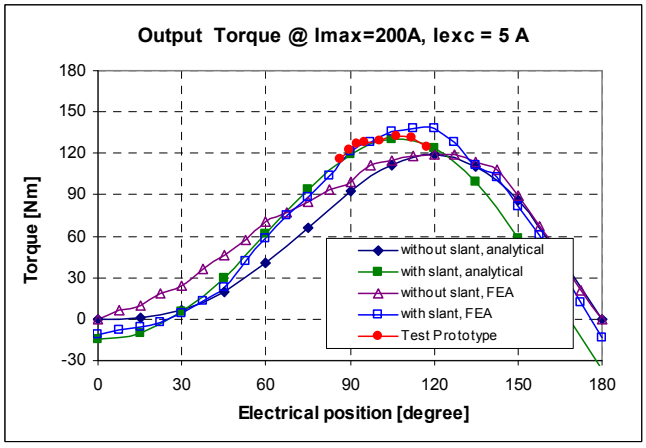

Fig. 10. Comparison of the expected output torque at I_{max}=200A.

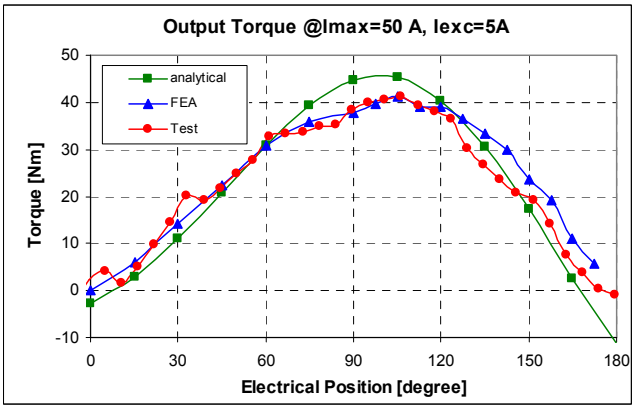

Fig. 11. Comparison of the expected output torque at I_{max}=50A.

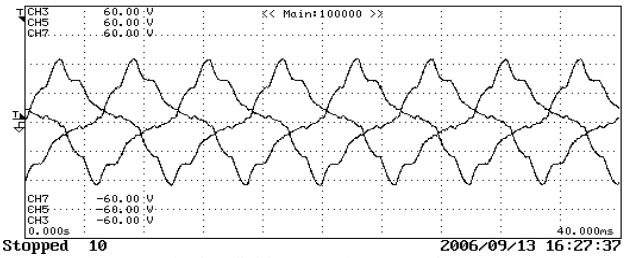

(a) No excitation field current (16.3 V_{rms}@1,000rpm)

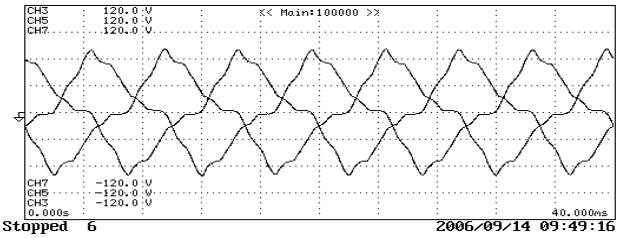

(b) 5A excitation field current (38 V_{rms}@1,000rpm)

Fig. 12. Comparison of the tested back emf voltage when the excitation current is 0 A and 5 A.

TABLE III
Comparison of simulation results in different air-gap models

	without slant	with slant	
	FEA	FEA	Test
Max.Reluctance torque @ I_{max}=200A	12.57 Nm	35.71 Nm	-
Max.Output torque @ I_{max}=200A, I_{exc}=5A	119.41 Nm	138.44 Nm	132.45 Nm
Back –emf * @ I_{exc}=5A	211.7 V	182.1 V	191.4 V
Back –emf * @ I_{exc}=0A	97.1 V	72.4 V	80.0 V
Back –emf ratio between I_{exc}=5A and I_{exc}=0A	2.18	2.52	2.39

* at 5000 rpm

VI. CONCLUSIONS

The experimental results of the prototype show the effects of the slanted air-gap. The summarized conclusions are as follows.

(1) The BFE structure achieves a higher ratio of controllable back-emf using the slanted air-gap.
(2) The maximum torque of the slanted air-gap rotor is higher than that of the uniform air-gap rotor (without slanted air-gap) in spite of the smaller air-gap flux.
(3) The slanted air-gap can be used in a conventional air-gap IPMSM for increasing its output torque.
(4) It is possible that the reduced PM flux could reduce the iron loss of the machine, especially at high-speed operation.
(5) For application of the slanted air-gap structure, it is necessary to study the harmonics in the air-gap flux caused by the unbalanced air-gap shape.

REFERENCES

[1] T. M. Jahns, "Component Rating Requirements for Wide Constant Power Operation of Interior PM Machine Drives," *IEEE Industry Applications Society*, **3**, 2000, pp. 1697 – 1704.

[2] A. M. El-Refaie and T. M. Jahns, "Comparison of Synchronous PM Machine Type for Wide Constant-Power Speed Range Operation," *IEEE Industry Applications Conference*, vol. 2, 2005, pp. 1015 –1022.

[3] J. S. Hsu, T. A. Burress, S. T. Lee, R. H. Wiles, C. L. Coomer, J. W. McKeever, and D. J. Adams, "16,000-rpm Interior Permanent Magnet Reluctance Machine with Brushless Field Excitation," ORNL/TM-2007/167, Oak Ridge National Laboratory, Oak Ridge, Tennessee, 2007.

[4] J. S. Hsu, S. T. Lee, R. H. Wiles, C. L. Coomer, K. T. Lowe, and T. A. Burress, "Effect of Side Permanent Magnets for Reluctance Interior Permanent Magnet Machines," *IEEE Power Electronics Specialists Conference*, Jun. 2007, pp. 2267 – 2272.

[5] J. S. Hsu, S. T. Lee, and L. M. Tolbert, "High-Strength Undiffused Brushless (HSUB) Machine," *IEEE Industry Applications Society*, Oct. 2008, pp. 1 – 8.

[6] J. S. Hsu, T. A. Burress, S. T. Lee, R. H. Wiles, C. L. Coomer, J.W. McKeever, and D. J. Adams, "16,000-RPM Interior Permanent Magnet Reluctance Machine with Brushless Field Excitation," *IEEE Industry Applications Society Annual Meeting*, Oct. 2008, pp. 1 – 6.

[7] T. J. E. Miller, *Brushless Permanent-Magnet and Reluctance Motor Drives*, London, Clarendon Press, 1989.

[8] S. A. Nasar, I. Boldea, and L. E. Unnewehr, *Permanent Magnet, Reluctance, and Self-Synchronous Motors*, CRC Press Inc., United States, 1993.

[9] M. A. Rahman, P. Zhou, "Analysis of Brushless Permanent Magnet Synchronous Motors," *IEEE Transactions on Industrial Electronics*, vol. 43, no. 2, 1996, pp. 256–267.

[10] I. Boldea, L. Tutelea, and C. I. Pitic, "PM-assisted reluctance synchronous motor/generator (PM-RSM) for mild hybrid vehicles: electromagnetic design," *IEEE Transactions on Industry Applications*, vol. 40, no. 2, March-April 2004, pp. 492 – 498.

[11] S. T. Lee, "Development and Analysis of Interior Permanent Magnet Synchronous Motor with Field Excitation Structure," Ph. D. dissertation, Dept. Elec. Eng., Univ. Tennessee, Knoxville, 2009.